

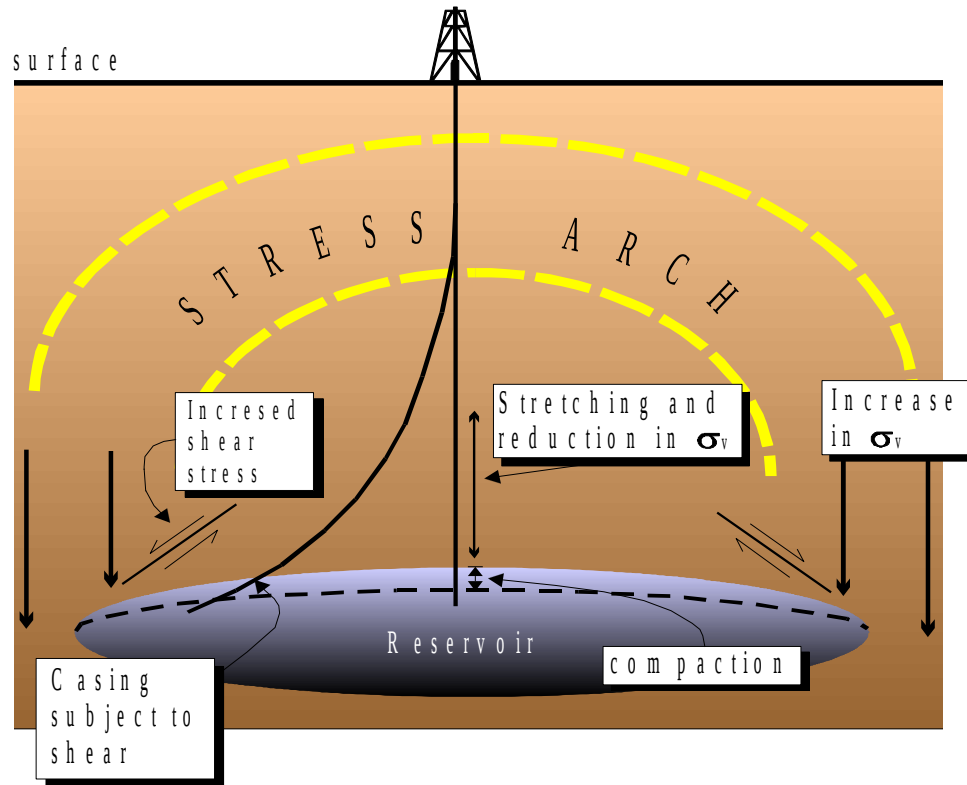
Acoustic Velocities of Shales: Stress and Frequency Dependence

Andreas Bauer, Dawid Szewczyk, Rune M. Holt

ROSE Meeting April 27-30, 2015

Stress dependence of seismic velocities

- Depletion / Inflation of reservoir results in stress changes in and around the reservoir, resulting in seismic-velocity and impedance changes.

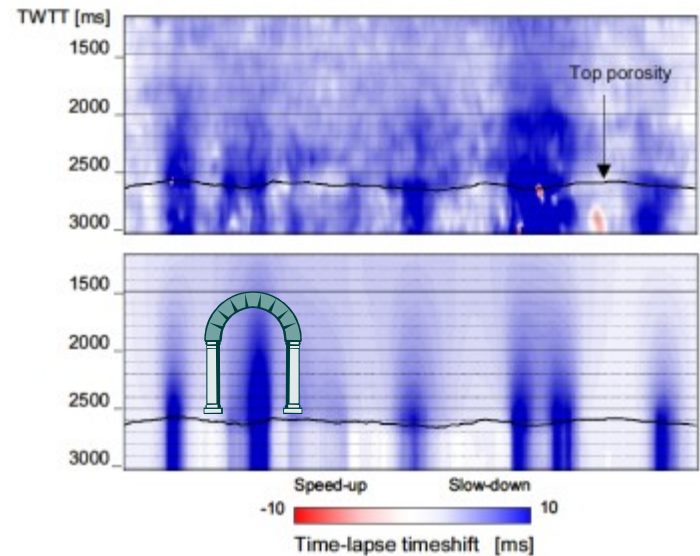


➤ Homogeneous, isotropic space $\Delta\bar{\sigma} = 0$ outside the reservoir

➤ Material contrast $\Delta\bar{\sigma} \neq 0$; $\Delta p_f \neq 0$

Stress dependence of seismic velocities

- Timelapse seismic data can be inverted for stress and strain changes in the subsurface (→ caprock integrity) and reservoir compaction (→ detection of undepleted pockets), provided that accurate geomechanical and rock physics models are available.
- Geomechanical model: links pore-pressure changes to stress and strain changes. Critical input parameters: geometry of lithologies and rock stiffnesses
- Rock physics model: links stress and strain changes to seismic velocity changes (rocks are non-linear elastic media!).



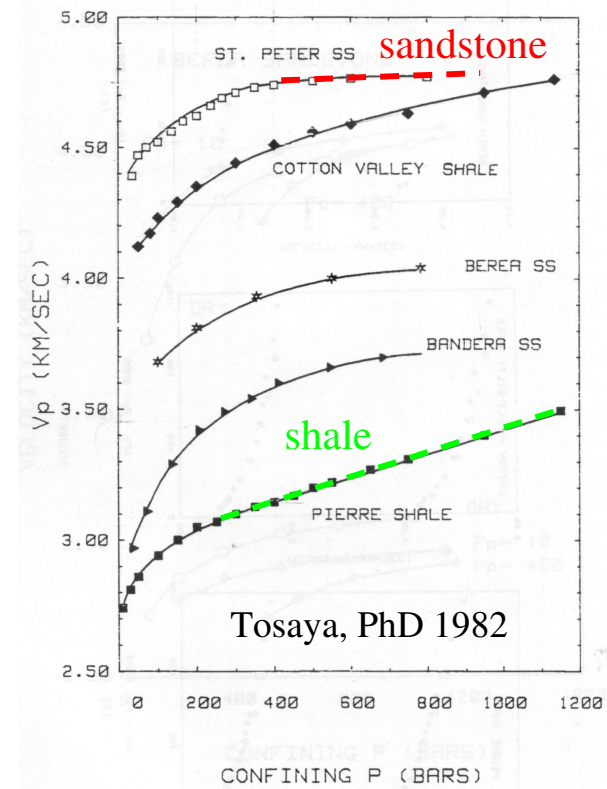
Hatchell & Bourne, 2005

Stress dependence of seismic velocities

Issues:

- How to obtain rock stiffnesses?
 - Reservoir rocks: Core material might be available
 - Overburden rocks (often shale): **stiffnesses obtained from seismic or sonic data using correlations. How good are those correlations?**

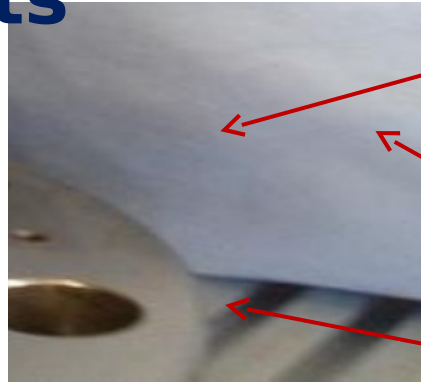
- How to obtain the stress and stress-path dependence of seismic velocities
 - Rock physics models often based on laboratory measurements at ultrasonic frequencies; dispersion effects are usually ignored
 - Recent tests with different types of shales show large seismic dispersion **👤 Better understanding of dispersion effects needed**



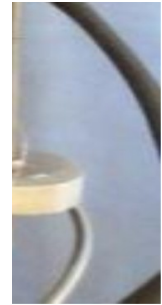
New compaction cell for seismic-dispersion measurements

measurements

- ❑ Compaction tests
- ❑ Control of confining stress, axial stress, and pore pressure
- ❑ Ultrasonic velocities, v_p , v_s
- ❑ Dynamic stiffness (Young's modulus, Poisson's ratio) at seismic frequencies (1 – 155 Hz)



Endcap with ultrasonic transducers (v_p , v_s) and pore-fluid line LVDT

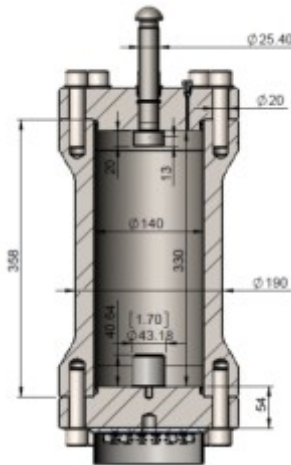


Rock sample (1" diameter) with 8 strain gages (4 axial, 4 radial) glued to it (rubber sleeve was removed)

Endcap with ultrasonic transducers (v_p , v_s) and pore-fluid line

Low-frequency unit consisting of piezoelectric actuator and piezoelectric force sensor

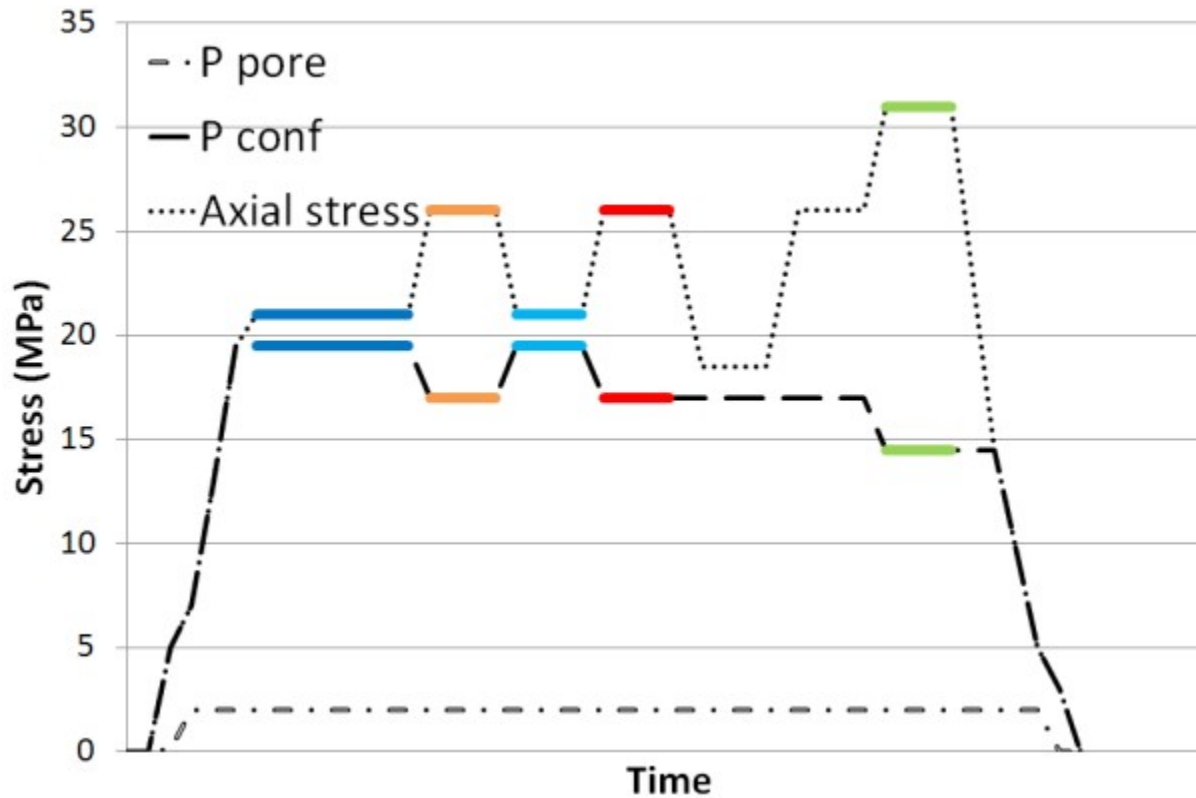
Internal load cell



Pierre shale: Stress dependence of

velocities

Stress path: Constant mean stress loading / unloading + triaxial unloading/loading



Pore fluid: brine
(3.5% NaCl)

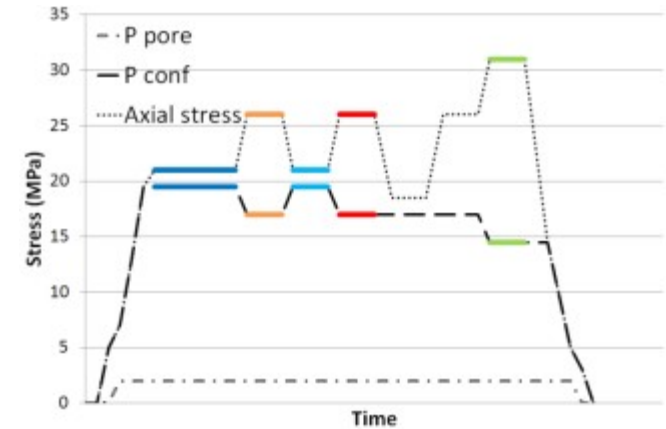
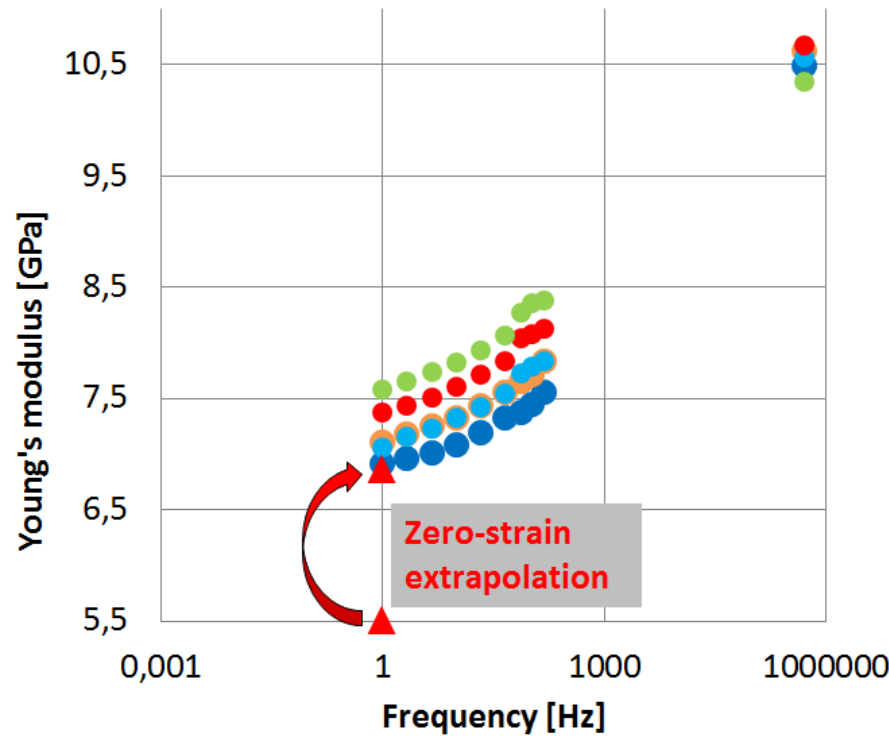
Use metal mesh for
side drainage



Change in deviatoric stress at constant mean stress corresponds to the stress path in the overburden and sideburden of a depleting / inflating reservoir for a homogeneous subsurface

Pierre shale: Stress dependence of

velocities Preliminary results



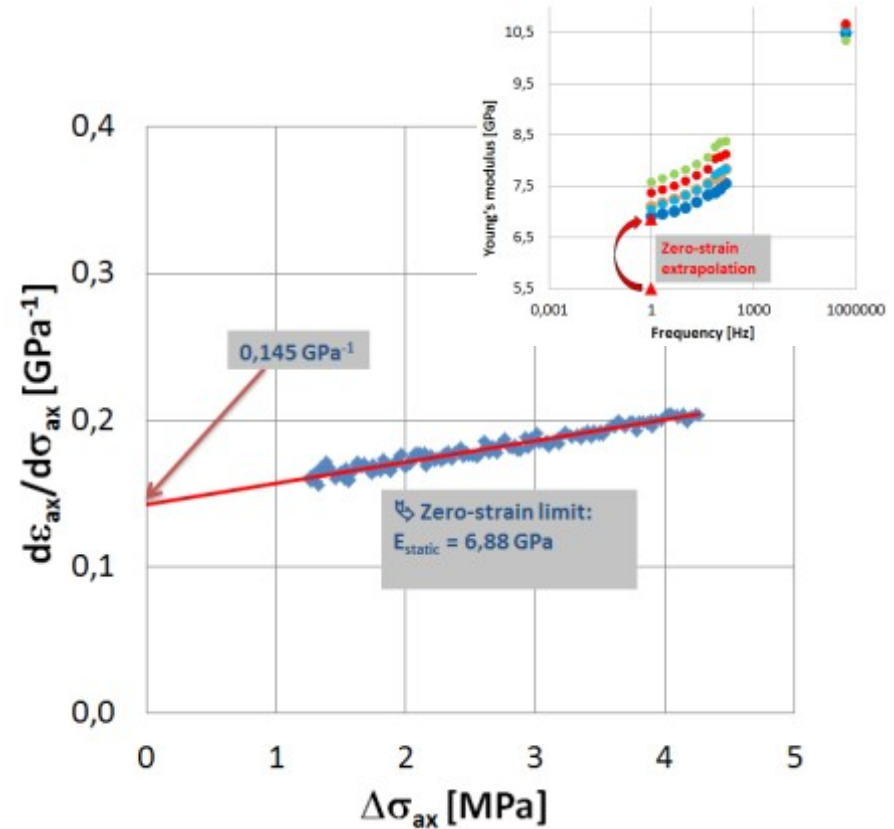
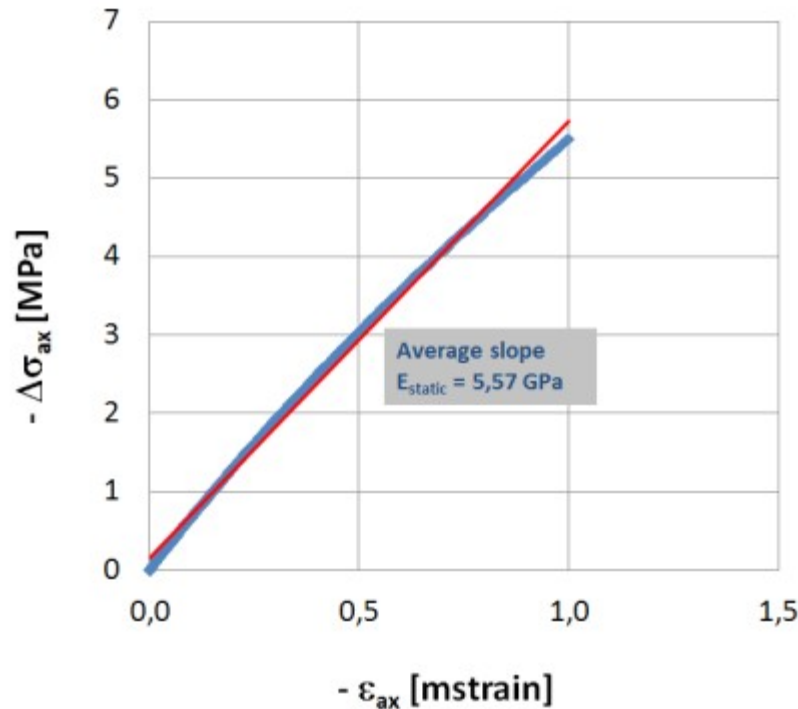
- Zero-strain static Young's modulus consistent with low-frequency measurements
- Seismic Young's modulus increases with increasing deviatoric stress
- Stress effects not fully reversible (due to plastic deformation, or experimental artefact?)
- Stress sensitivity is different for seismic and ultrasonic frequencies, and even changes sign at high deviatoric stress

Pierre shale: Stress dependence of velocities

Zero-strain limit of static Young's modulus

Static Young's modulus has elastic and non-elastic component
 During triaxial unloading, the non-elastic component vanishes in the limit of zero strain
 Assumption (proven for sandstones)*: $d\varepsilon_{ax}/d\sigma_{ax}$ increases linearly with $\Delta\sigma_{ax}$

* Fjær, Stroisz, Holt, ARMA 12-537 (2012)



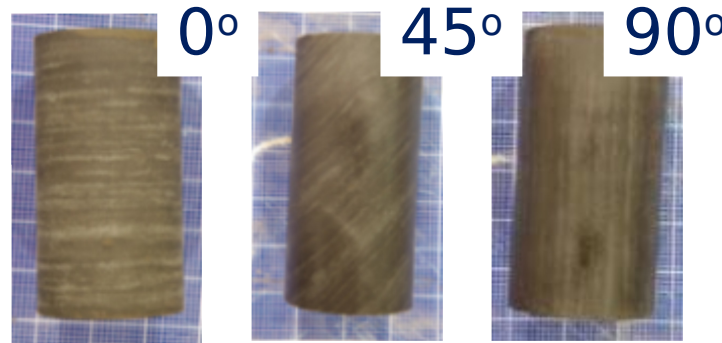
Mancos shale: Stress dependence of

velocities

- Three sample orientations (allowing for the determination of all 5 independent stiffness-matrix components: C_{11} , C_{33} , C_{44} , C_{66} , C_{13})

$$\bar{C} = \begin{pmatrix} C_{11} & C_{12} & C_{13} & 0 & 0 & 0 \\ C_{12} & C_{11} & C_{13} & 0 & 0 & 0 \\ C_{13} & C_{13} & C_{33} & 0 & 0 & 0 \\ 0 & 0 & 0 & C_{44} & 0 & 0 \\ 0 & 0 & 0 & 0 & C_{44} & 0 \\ 0 & 0 & 0 & 0 & 0 & C_{66} \end{pmatrix}$$

with $C_{66} = \frac{1}{2}(C_{11} - C_{12})$



Samples were tested as received; no pore-pressure control (saturation state corresponds to a rel. humidity of $\approx 86\%$)

$$\rho_{PP} = \rho V_{PV}^2; \quad C_{11} = \rho V_{PH}^2; \quad C_{44} = \rho V_{SV}^2; \quad C_{66} = \rho V_{SH}^2$$

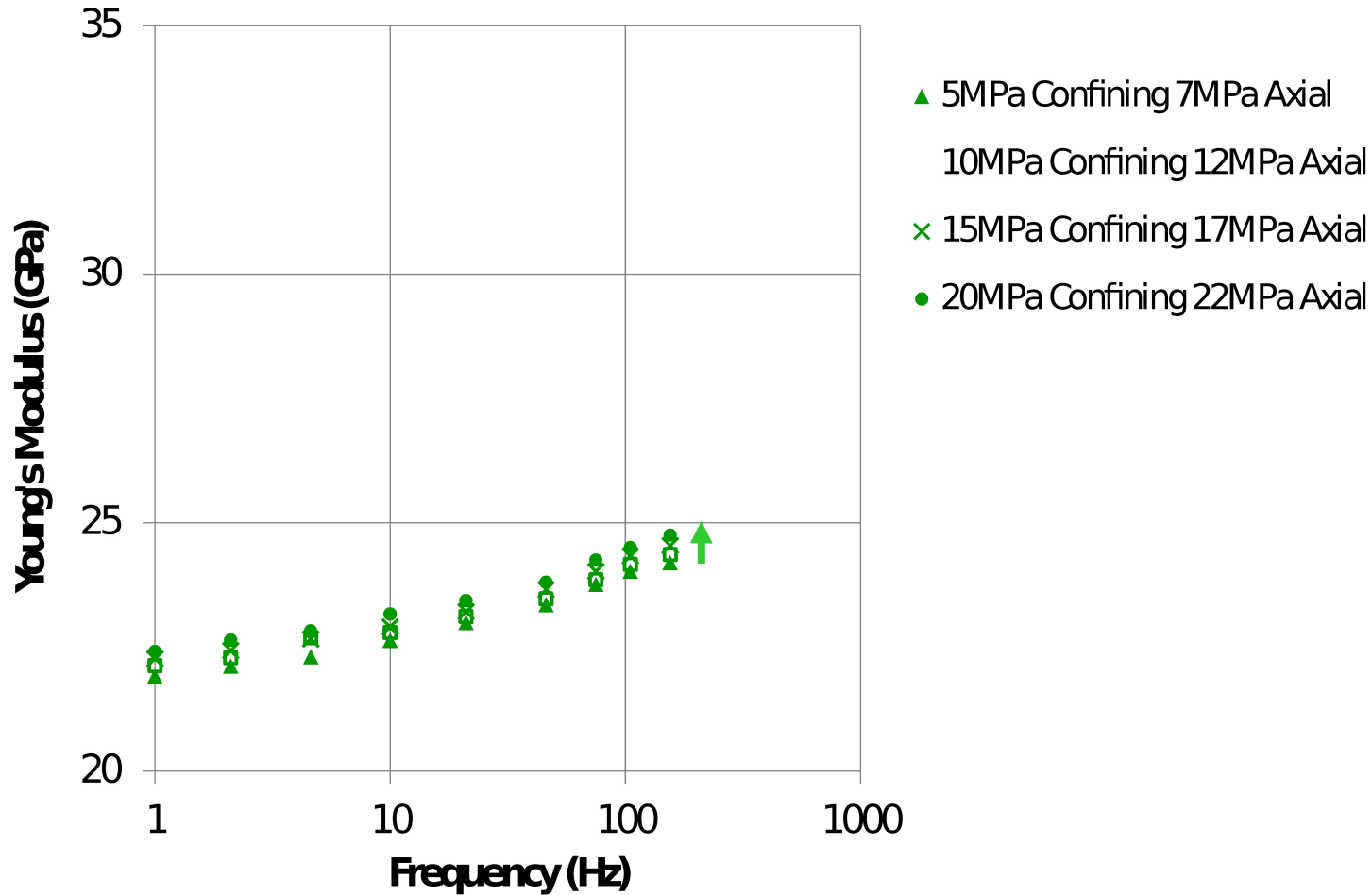
$$C_{13} = \frac{\sqrt{(2V_{qP}^2 - V_{PH}^2 \sin^2 \theta - V_{PV}^2 \cos^2 \theta + V_{SV}^2)^2 - ((V_{PH}^2 - V_{SH}^2) \sin^2 \theta - (V_{PV}^2 - V_{SV}^2) \cos^2 \theta)^2}}{2 \sin \theta \cos \theta} + V_{SV}^2$$

Stress states:

- $P_{\text{conf}} = 5 \text{ Mpa}$, $\sigma_{\text{ax}} = 7 \text{ MPa}$
 - $P_{\text{conf}} = 10 \text{ Mpa}$, $\sigma_{\text{ax}} = 12 \text{ MPa}$
 - $P_{\text{conf}} = 15 \text{ Mpa}$, $\sigma_{\text{ax}} = 17 \text{ MPa}$
 - $P_{\text{conf}} = 20 \text{ Mpa}$, $\sigma_{\text{ax}} = 22 \text{ MPa}$
- Comment: A constant deviatoric stress of 2 MPa was applied in axial direction in order to improve the signal quality of the low-frequency data; the impact of this deviatoric stress on the rock stiffness was ignored in the anisotropy analysis, which is justified since the angular dependence of the velocities is much larger than the stress effect.

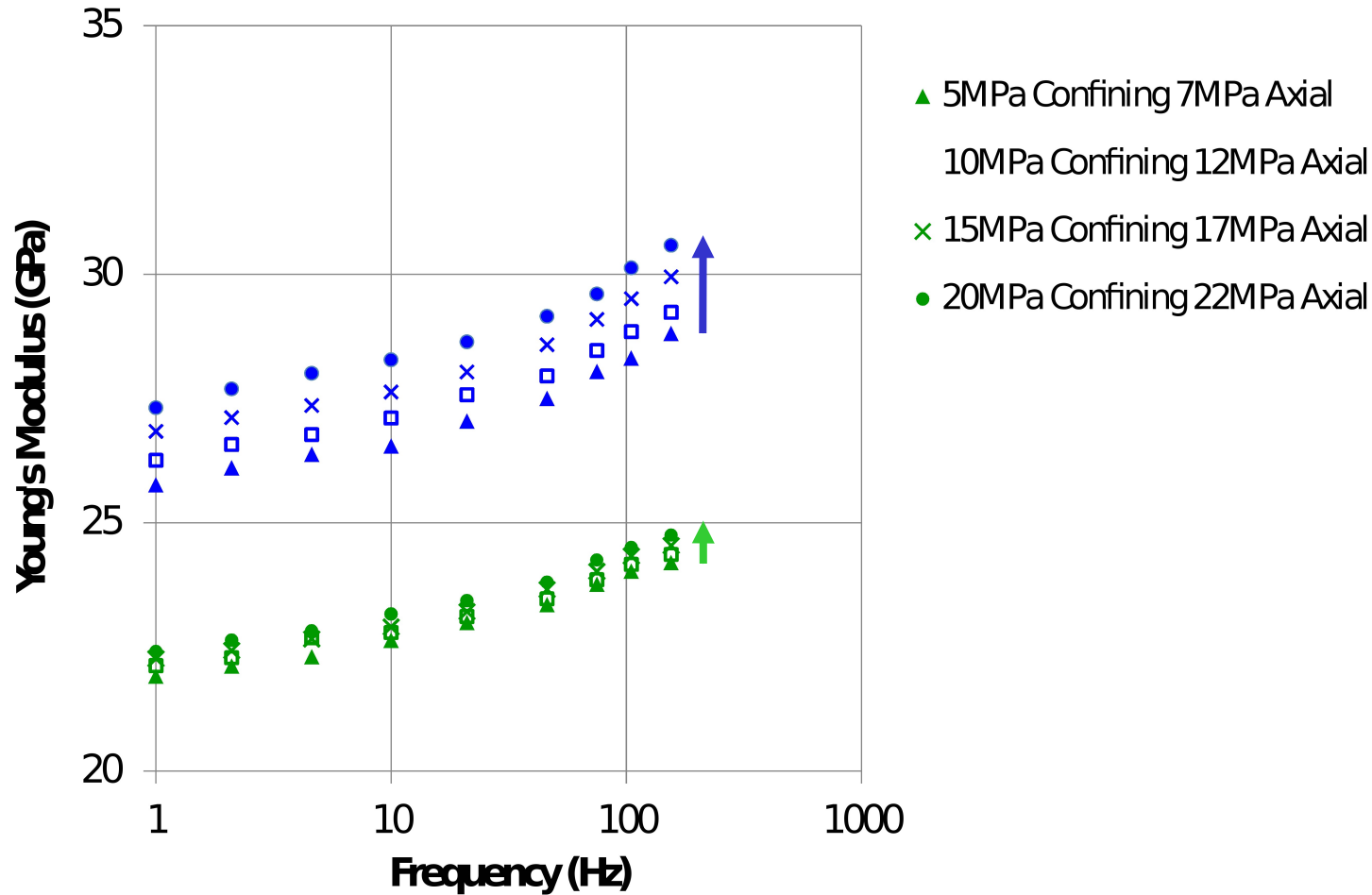
Mancos shale: Stress dependence of velocities

Results of low-frequency measurements



Mancos shale: Stress dependence of velocities

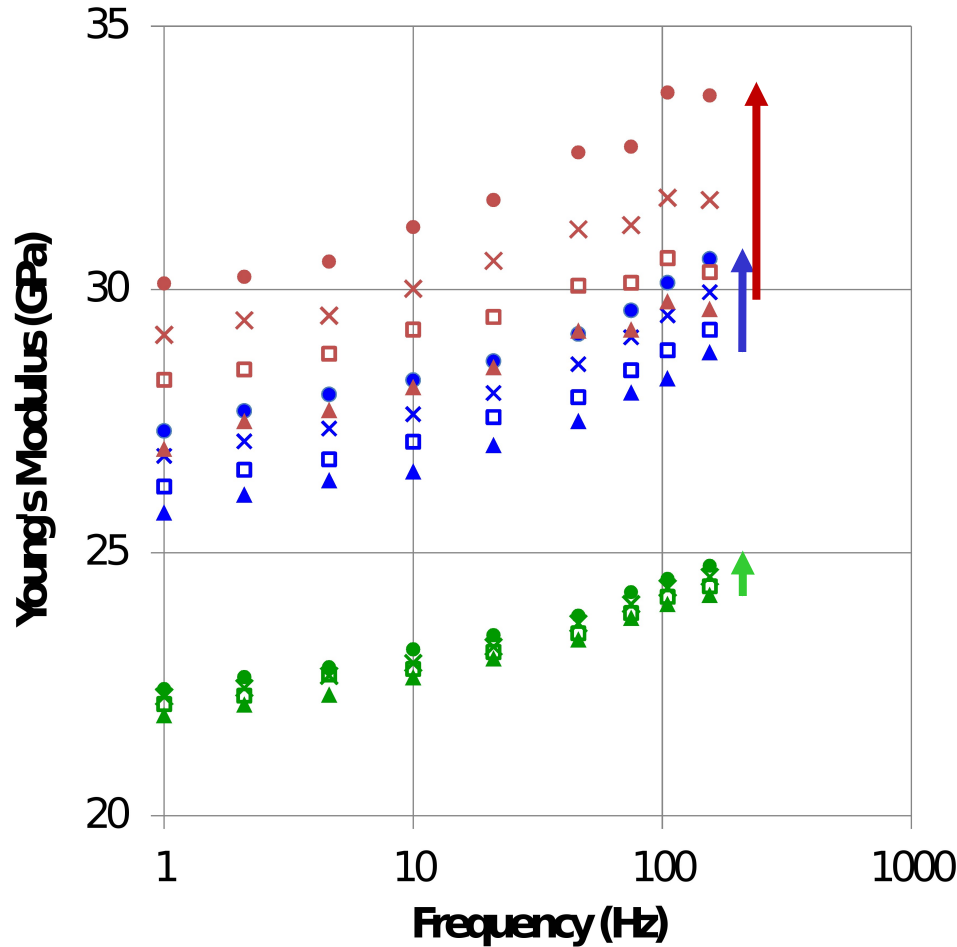
Results of low-frequency measurements



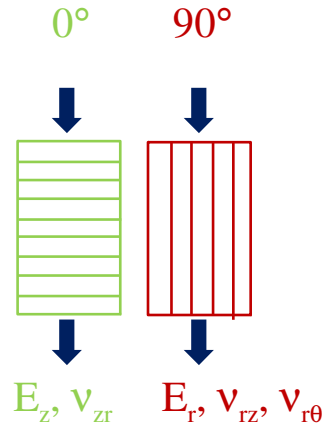
Manco shale: Stress dependence of

velocities

s of low-frequency measurements - Youngs-modulus

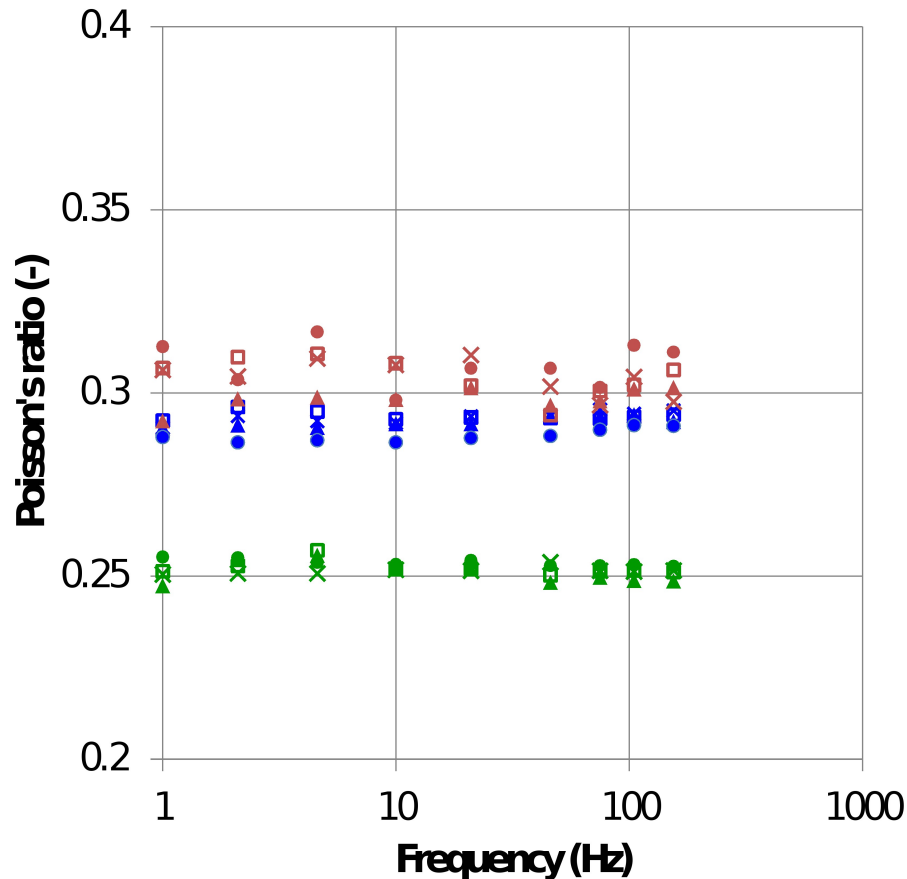


- ▲ 5MPa Confining 7MPa Axial
- 10MPa Confining 12MPa Axial
- × 15MPa Confining 17MPa Axial
- 20MPa Confining 22MPa Axial

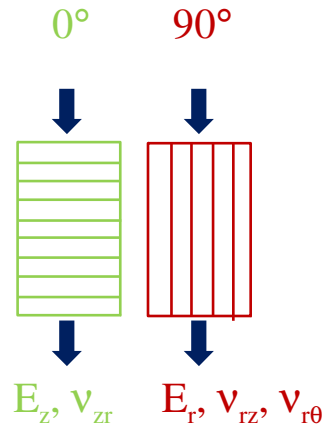


- Significant dispersion within seismic band
- Increase in confining stress results in stiffening of the rock
- Stress dependence strongly depends on sample orientation

Manco shale: Stress dependence of velocities of low-frequency measurements - Poisson's ratio (average)



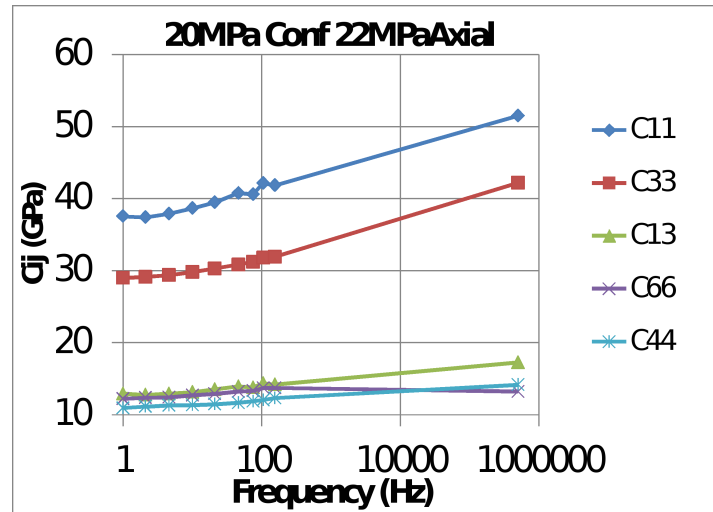
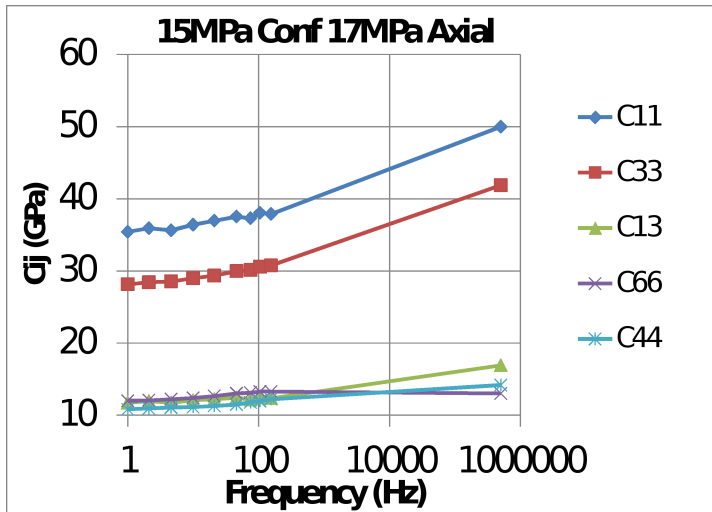
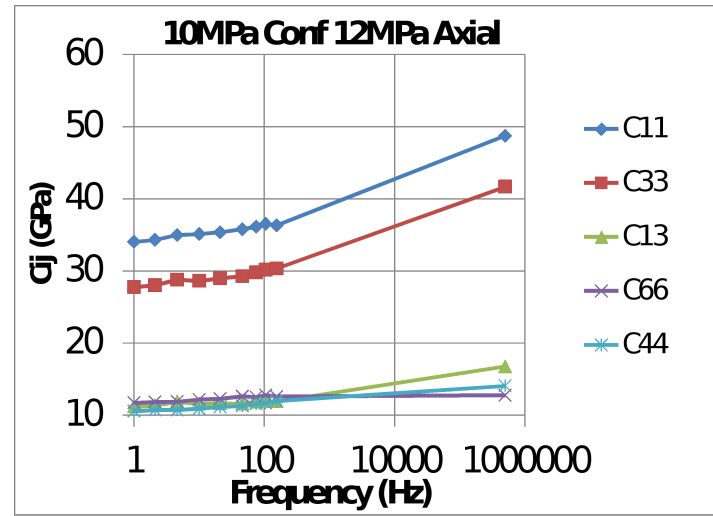
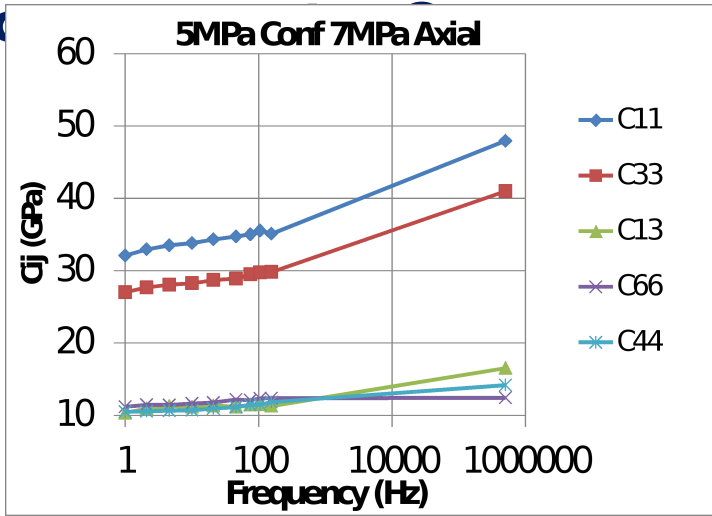
- ▲ 5MPa Confining 7MPa Axial
- 10MPa Confining 12MPa Axial
- × 15MPa Confining 17MPa Axial
- 20MPa Confining 22MPa Axial



- **Negligible dispersion within seismic band**
- **Poisson's ratio depends on sample orientation**

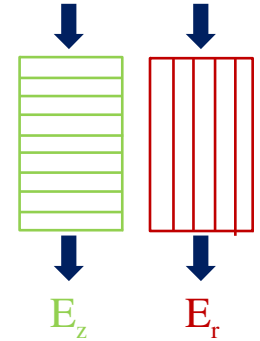
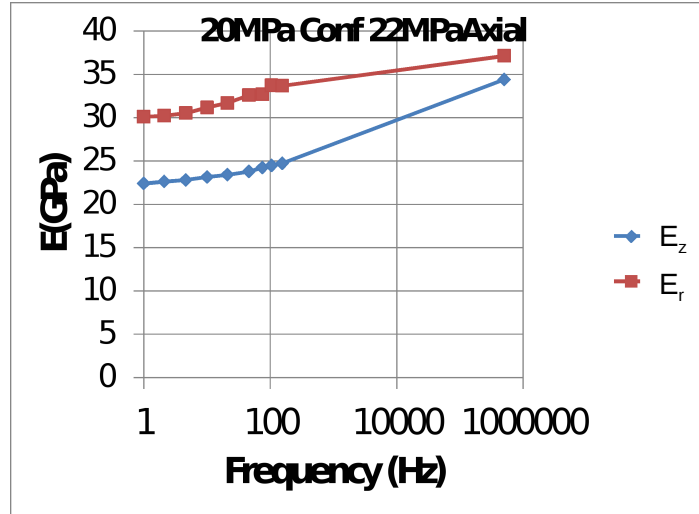
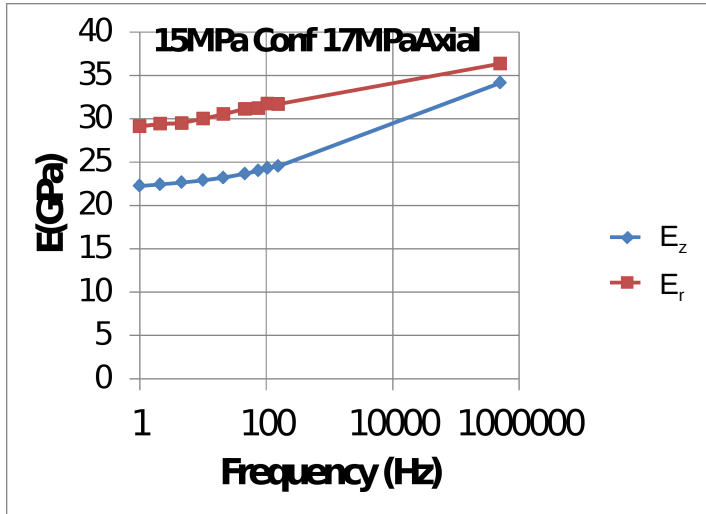
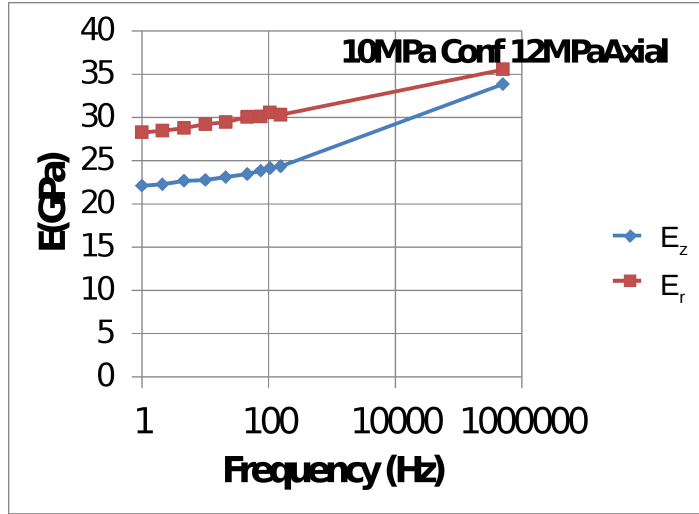
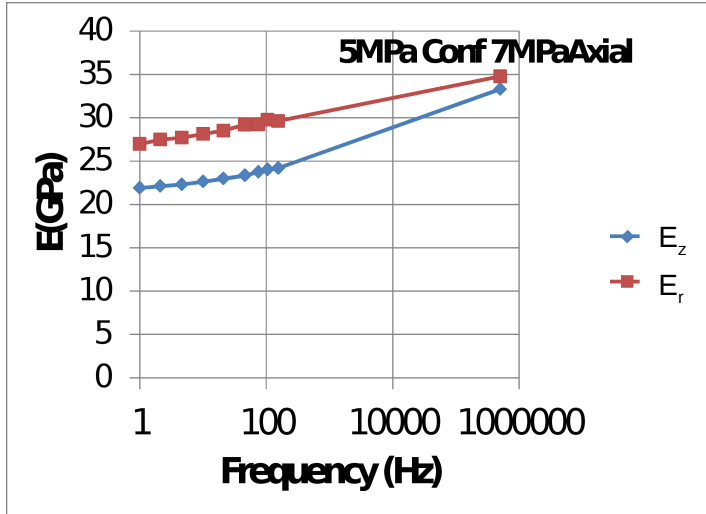
Manco shale: Stress dependence of

Velocities combined low-frequency and ultrasonic measurements - Dispersion Stiffness matrix



Manco shale: Stress dependence of

Velocities combined low-frequency and ultrasonic measurements - Young's moduli, E_z , E_r

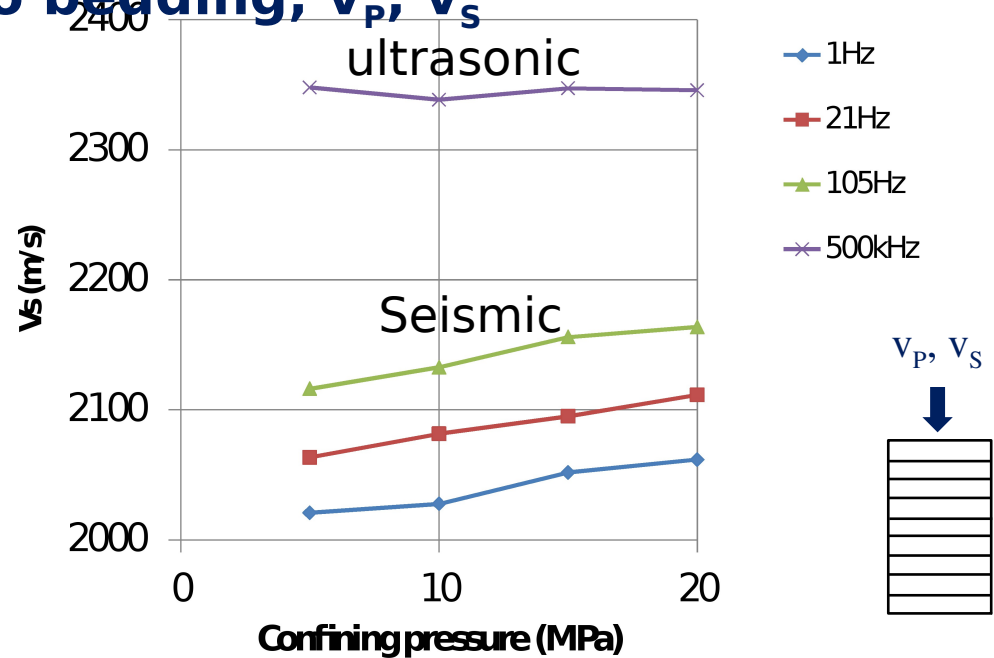
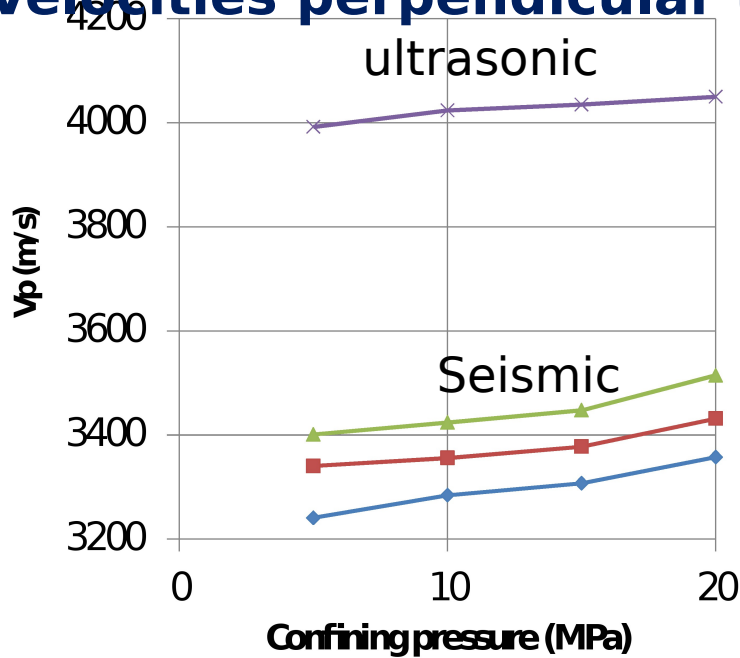


Significantly larger difference in E_z and E_r at seismic frequencies

Mancoos shale: Stress dependence of


Velocities combined low-frequency and ultrasonic measurements -

Velocities perpendicular to bedding, v_p , v_s



- Larger stress dependence of v_p and v_s at seismic frequencies
- v_s at ultrasonic frequencies exhibits negligible change with stress, while v_s at seismic frequencies increases gradually with stress
- Preliminary results only! Anisotropy data needs to be checked for consistency

Summary

- ❑ **Shales, both fully saturated (Pierre) and partially saturated (Mancos), exhibit significant seismic dispersion**
- ❑ **Dispersion mechanism in shales not yet understood**
- ❑ **Seismic dispersion in shales is strongly affected by stress**
- ❑ **Stress dependence of v_p and v_s is not the same at seismic and ultrasonic frequencies**  **Rock physics models based on ultrasonic data may not apply**
- ❑ **Shale anisotropy has to be taken into account**
- ❑ **More experimental studies and improved rock-physics models needed**